Research Article

Pushing it to the Limit: Adaptation with Dynamically Switching Gain Control

Matthias S. Keil[1] and Jordi Vitrià[1, 2]

[1] *Centre de Visiò per Computador, Edifici O, Campus UAB, 08193 Bellaterra, Cerdanyola, Barcelona, Spain*
[2] *Computer Science Department, Universitat Autònoma de Barcelona, 08193 Bellaterra, Cerdanyola, Barcelona, Spain*

With this paper we propose a model to simulate the functional aspects of light adaptation in retinal photoreceptors. Our model, however, does not link specific stages to the detailed molecular processes which are thought to mediate adaptation in real photoreceptors. We rather model the photoreceptor as a self-adjusting integration device, which adds up properly amplified luminance signals. The integration process and the amplification obey a switching behavior that acts to shut down locally the integration process in dependence on the internal state of the receptor. The mathematical structure of our model is quite simple, and its computational complexity is quite low. We present results of computer simulations which demonstrate that our model adapts properly to at least four orders of input magnitude.

1. INTRODUCTION

There is agreement that adaptation (i.e., the adjustment of sensitivity) is important for the function of nervous systems, since without corresponding mechanisms, any neuron with its limited dynamic range would stay silent or operate in saturation most of the time [1]. Because neurons are noisy devices, reliable information transmission is only granted if the distribution of levels in the stimulus matches the neuron's reliable operation range [2].

Consider, for example, the mammalian visual system, with the retina at its front end. When performing saccades, the retina must cope with intensity variations which may span about one [3, 4] to about two orders of magnitude (2 including shadows according to [3], 2-3 according to [5]). From one scene to another (e.g., from bright sunlight to starlight), the range of intensity variations may well span up to ten orders of magnitude [6–9]. This range of intensities has to be mapped onto less than two orders of output activity of retinal ganglion cells [10], implying some form of compression of the scale of intensity values. The retina achieves this by making use of a cascade of gain control and adaptation mechanisms, respectively (e.g., [11–14]). Specifically, cone photoreceptors may decrease their sensitivity proportionally to background intensity, over

about 8 log units of background intensity [15]. This relationship is known as Weber's law (e.g., [16]). Adaptation in photoreceptors is achieved by subtly balanced network of molecular processes (see [17] for an excellent introduction, and [14, 18] with references). Many of the data were gained from rod photoreceptors because they are more amenable to analysis. It is generally believed, however, that similar processes are also taking place in cones.

With the present paper, we propose a mechanism which mimics the dark and light adaptations of retinal cones. Our mechanism abstracts from the detailed molecular processes of the transduction cascade as described in the following section. We seeked out an easy implementable and computationally efficient way of achieving the adaptation behavior of cone photoreceptors. Our approach should—and will be—contrasted with the retinal stage of a recently proposed model of Grossberg and Hong [19, 20], which simulates (i) luminance adaptation at the outer segment of the photoreceptor (cf. [21]), and (ii) inhibition at the inner segment of the photoreceptor by horizontal cells (e.g., [22]). In their model, horizontal cells are coupled with gap junctions (forming a syncytium), whose connectivity or permeability decreases with increasing differences between the inputs of adjacent cells [23, 24]. In other words, their horizontal cell network establishes current flows inside of regions that are

defined by low contrasts, whereas no activity exchange occurs between regions which are separated by high contrast boundaries (very similar to an anisotropic diffusion mechanism [25]). In this way, contrast adaption is implemented. Notice that our model lacks the latter stage, and only simulates the photoreceptor adaptation.

2. MECHANISMS OF ADAPTATION IN THE RETINA

A response to light is initiated by photoisomerization of the chromophore 11-*cis*-retinal to all-*trans*-retinal. In darkness, 11-*cis*-retinal is bound to rhodopsin in its inactive conformation, and lies buried in the membranes of the outer segment discs. Upon absorption of a photon, and the subsequent photoisomerization of the chromophore, the rhodopsin undergoes a conformational change which converts it into its active form Rh^* (or metarhodopsin II). The presence of Rh^* triggers two distinct mechanisms: a recycling process known as visual cycle, and an enzymatic cascade known as transduction cascade.

The visual cycle begins with the phosphorylation of Rh^*, and subsequent binding of arrestin to the phosphorylated photopigment. After, binding of arrestin, the photopigment is rendered completely inactive. The protein opsin is then dephosphorylated, and all-*trans*-retinal is reduced to all-*trans*-retinol. The retinol is isomerized to the 11-*cis*-isomer outside the photoreceptor (in the adjacent retinal pigment epithelium layer), and reenters afterwards to recombine with the dephosphorylated opsin.

The transduction cascade begins with the serial activation of transducins by Rh^*, implementing the first stage for signal amplification in the cascade [26]. Thereby, an active complex $T_\alpha \cdot GTP$ is formed, which binds to and activates the enzyme phosphodiesterase (PDE). PDE reduces the concentration of cytoplasmatic cGMP by hydrolizing it. The latter process constitutes a second stage for amplification. The hydrolysis of cGMP causes the closing of cGMP-gated channels, what in turn generates the electrical response of photoreceptors. Thus, photoreceptors are depolarized in darkness because of their open cationic channels, and get hyperpolarized by light. In darkness, the steady current that flows into the outer segment is usually called dark or circulating current.[1] The main fraction of the circulating current is carried by Na^+ ions, and a smaller fraction of Ca^{2+} ions [27]. Calcium is transported out of the outer segment by the Na^+/K^+-Ca^{2+}-exchange protein at a constant rate, independent of the light hitting the photoreceptor. This implies that light decreases intracellular Ca^{2+} levels, because of the increased probability of channel opening. As a consequence, a direct correlation (i.e., a linear relationship) exists between the circulating current and Ca^{2+} concentration.

Adaptation of the photoreceptor to ambient light is granted by balancing the just described amplification mechanisms (for low light situations) against mechanisms which prevent response saturation (e.g., for sunlit scenes). This balance is implemented by feedback mechanisms which act either on the catalytic activity or on the catalytic lifetime of the components that make up the phototransduction cascade [28]. It is now well established that changes in Ca^{2+} concentration regulate the cascade in at least three important ways.

First, Ca^{2+} can prolong the lifetime of Rh^* through the inhibition of phosphorylation in the visual cycle, by means of recoverin. Second, in the transduction cascade, Ca^{2+} regulates the cytoplasmatic concentration of cGMP by binding to guanylate cyclase—the enzyme that is responsible for cGMP synthesis. Third, decreasing Ca^{2+} concentrations increases the sensitivity of the cationic channels to cGMP [29].

Taken together, Ca^{2+} is now considered as the photoreceptor's internal messenger for adaptation. Supporting evidence comes from the fact that adaptation effects can be provoked without light (cf. [14, page 130]), by only lowering the Ca^{2+} concentration, or that adaptation is suspended by clamping the Ca^{2+} level to its value corresponding to darkness (see [14, page 126]).

Beyond the level of the individual photoreceptor, further mechanisms related to adaptation are effective, for example network adaptation in interneurons and retinal ganglion cells (i.e., adaptation is "transferred" beyond the receptive field of the actually stimulated cell, e.g., [30–33]), and discounting predictable spatio-temporal structures from the stimulus by Hebbian mechanisms [34, 35].

3. FORMAL DEFINITION OF THE ADAPTATION DYNAMICS

Table 1 gives a brief comparison of components, and a sketch of our model is shown in Figure 1. In what follows, we give the formal introduction to our mechanisms which are thought to provide an abstract view for adaptation as it takes place in the outer segment of individual photoreceptors.

Let $\mathcal{L}_{ij}$ be a two-dimensional luminance distribution which provides the input into our model. For the purpose of the present paper, we assume that the model converges before changes in luminance occur, that is, $\partial \mathcal{L}_{ij}(t)/\partial t = 0$, where spatial coordinates are denoted by (i, j). We assume that the input is normalized according to $\epsilon < \mathcal{L} \leq 1$, with ϵ is chosen such that $0 < \epsilon < \min_{i,j}\{\mathcal{L}_{ij}\}$. Let P denote the membrane potential of the photoreceptor, which is assumed to obey the equation (the symbols g_{leak}, $g_{\text{exc}}(t)$, and V_{exc} are defined below)

$$\frac{dP(t)}{dt} = -g_{\text{leak}}P(t) + g_{\text{exc}}(t)[V_{\text{exc}} - P(t)]. \quad (1)$$

Table 1: *Model overview*: an overview over the mechanisms used in the model of Grossberg and Hong [19, 20] and our approach.

Mechanism	[19, 20]	Our approach
Light adaptation	Yes	Yes
Local divisive gain control	No	Yes

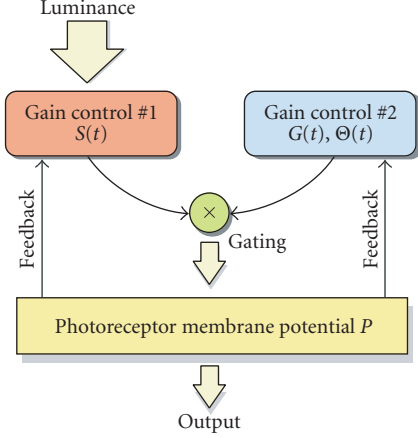[1] The photocurrent is brought back to the dark-adapted level by hydrolizing the GTP to GDP.

FIGURE 1: *Model sketch*: a luminance distribution is subjected to a divisive "gain control" stage #1 ($S(t)$, (3)). At this stage, inhibition of luminance $\mathcal{L}$ takes place as a function of increasing photoreceptor potential P. The second gain control stage $G(t)$ can either amplify the signal $S(t)$ or attenuate it ((4), (5), and (6)). Amplification of $S(t)$ occurs if the membrane potential P falls below a threshold Θ, and attenuation for $P > \Theta$ (see (5)). Both "gain control" stages interact multiplicatively (denoted by the symbol "$\otimes$," (2)) before providing excitatory input into the photoreceptor's membrane potential (symbol "P," (1)). The photoreceptor potential in turn feeds back into both of the "gain control" stages. At the same time, the photoreceptor potential represents the output of our model.

TABLE 2: *Simulation details*: the table is self-explanatory. For the integration of (1), a fourth-order Runge-Kutta scheme was used with an integration time step of 0.01. The remaining differential equations were integrated with Euler's method with an integration time step of one. Notice that the integration step sizes were not adjusted to match physiological time scales.

Parameter	Value	Equation	Description
g_{leak}	0.05	(1)	Leakage conductance
V_{exc}	1	(1)	Synaptic battery
γ	1.5	(3)	Divisive gain
τ_1	0.7213	(5)	Damping time constant
τ_2	−40.4979	(5)	Amplification time constant
Θ_0	0.25	(6)	Initial threshold value
τ_Θ	39.4949	(6)	Threshold decay time constant

An instance of the last equation holds for each position (i, j), hence $P \equiv P_{ij}(t)$ (in what follows, indices were dropped for brevity). The excitatory saturation point (or reversal potential) is defined by V_{exc}, and the leakage (or passive) conductance is defined by g_{leak} (note that V_{exc} represents an asymptote for P). Both of the last constants are equal for all photoreceptor cells. The default simulation parameters, as well as further simulation details, can be found in Table 2. Notice that photoreceptors in fact hyperpolarize in response to light (cf. Section 2), whereas the last equation makes a contrary assumption. This assumption, however, implies no loss of generality, since the model can equivalently be reformulated such that it hyperpolarizes with increasing intensity levels.
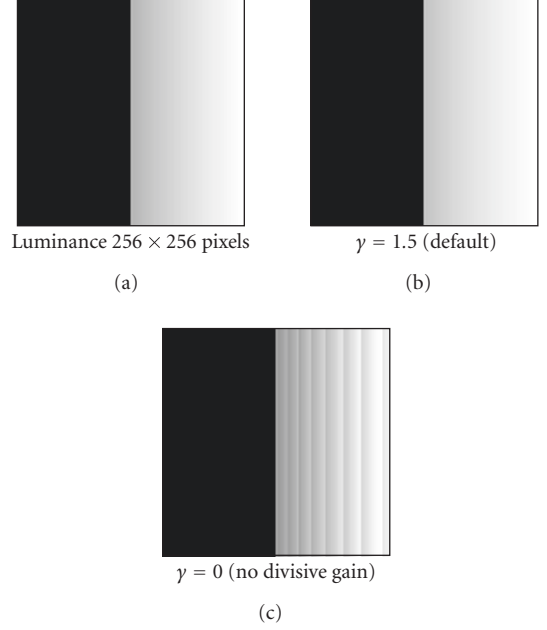

Luminance 256 × 256 pixels

(a)

$\gamma = 1.5$ (default)

(b)

$\gamma = 0$ (no divisive gain)

(c)

FIGURE 2: *Artifacts with a luminance ramp*. (a) The input $\mathcal{L}_{ij}$, a luminance step with a superimposed luminance ramp (increasing linearly from left to the right). (b) With the default value $\gamma = 1.5$ in (3), the adapted image is correctly rendered and hardly distinguishable from the input. (c) Setting $\gamma = 0$ causes the appearance of ripple artifacts in the adapted image. All results are shown at $t = 250$ iterations.

Excitatory input to the photoreceptor potential is given by the conductance $g_{exc} \equiv g_{exc,ij}(t)$, which is defined by

$$g_{exc}(t) = G(t) \cdot S(t), \qquad (2)$$

where the process $G \equiv G_{ij}(t)$ interacts multiplicatively with the light-induced signal $S \equiv S_{ij}(t)$ (such interaction was previously referred to as mass action or gating mechanism, see [21]). For the signal S, we assume that its efficiency for driving the photoreceptor's potential diminishes with increasing potential P:

$$S(t) = \frac{\mathcal{L}}{1 + \gamma \cdot P(t)}. \qquad (3)$$

The last equation in fact establishes a feedback mechanism which allows the photoreceptor to regulate the strength of its own excitatory input. In addition, the excitatory drive of the photoreceptor is also a decreasing function of increasing potential $P(t)$ by virtue of the term "$(V_{exc} - P)$" (the driving potential) in (1). Notice that if g_{exc} was constant and sufficiently high, the driving potential would make $P(t)$ saturate at V_{exc} (i.e., V_{exc} is asymptotically approached). Therefore, both the excitatory input g_{exc} and the driving potential decrease as $P(t)$ grows. The motivation for including (3) in our model was to eliminate ripple artifacts seen with luminance ramps (Figure 2). With "normal" natural images, those artifacts did not appear to be a major nuisance (Figure 3, see also Section 4).

$G(t) = 1$ (constant)

(a)

$\gamma = 0$ (no divisive gain)
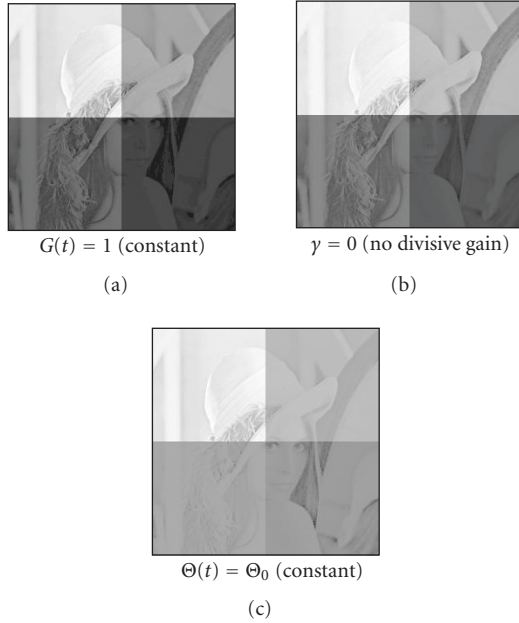
(b)

$\Theta(t) = \Theta_0$ (constant)

(c)

FIGURE 3: *Artifacts*: the results shown in this figure should be compared with Figure 7. (a) Setting the amplification constant to $G(t) = 1$ in (2) diminishes adaptation (i.e., low luminance values are not pushed that high). Notice that in this case dynamical switching is made inoperative. (b) Setting $\gamma = 0$ in (3) has no effect on the *natural* images we have tested, but causes strong ripple artifacts with luminance ramps as demonstrated in Figure 2. (c) Using a constant threshold $\Theta(t) = \Theta_0 = 0.25$ in (5) leads to strong saturation (or over-adaptation). All results are shown at $t = 250$ iterations.

The process $G(t)$ implements an amplification mechanism as follows:

$$\tau_k \frac{dG(t)}{dt} = -G, \qquad (4)$$

where the initial condition $G(t = t_0) = 1$ was used. Simulations are assumed to start at $t_0 = 0$. By virtue of the index $k \in \{1, 2\}$ associated with the time constant τ_k, the last equation describes *two* distinct processes. These processes are characterized by $\tau_1 > 0$ (making G decay with time), and $\tau_2 < 0$ (leading to an increase of G with time). The last equation thus implements what we dubbed a "dynamically switching gain control." But who or what is switching G on (i.e., making it increase with $|\tau_2|$) or off (i.e., making it decrease with τ_1)? The one or the other process is invoked depending on whether P exceeds a threshold Θ or not:

$$\begin{aligned} k &= 1 \quad \text{if } P(t) > \Theta(t), \\ k &= 2 \quad \text{otherwise.} \end{aligned} \qquad (5)$$

This means that if the outer segment potential P is below the threshold Θ, its input $g_{\text{exc}}(t)$ is amplified via (3). The amplification mechanism acts to diminish the integration time of luminance signals until reaching the threshold Θ, especially low-intensity signals. Once the threshold is exceeded, amplification is switched off (Figure 5). In fact, G decays rapidly

then in order to avoid driving the outer segment potential into saturation (which nevertheless may occur at sufficiently high intensity values). With ineffective dynamical switching $G \equiv$ const adaptation is severely deteriorated (Figure 3(a)). Mathematically, the dynamic switching mechanism avoids an unbounded growth of G.

Amplification proceeds until P crosses a threshold. The threshold, however, is not fixed, but is rather represented by a slowly decaying process on its own:

$$\tau_\Theta \frac{d\Theta(t)}{dt} = -\Theta(t). \qquad (6)$$

We used the initial condition $\Theta(t = t_0) = \Theta_0$, and like to point out that the threshold Θ is not supposed to represent a firing threshold for the photoreceptor. It rather serves to implement the dynamic switching behavior for turning the signal amplification on or off. The motivation for including a dynamical threshold in our model was the elimination of artifactual contrasts inversion effects, and will be explained in more details in Section 4. Furthermore, if a constant threshold was chosen, over-adaptation would occur (Figure 3(c)).

Our simulations were evaluated at the moment when $P_{ij} > \Theta_{ij}$ for all (i, j). This is, however, not a steady state, because the outer segment potential continues to decay with g_{leak}. The results which are presented in Figures 8 to 10 therefore show snapshots of the outer segment potential at exactly the moment when the last potential value $P_{ij}(t)$ exceeded the threshold $\Theta(t)$ (i.e., (i, j) corresponds to the position with the lowest intensity value in the input).

One may ask why we gave preference to a dynamical formulation of our model over steady state equations. Intuitively, steady state solutions cannot capture the full behavior revealed by the model. For example, the steady state solution (as defined by $d\Theta/dt = 0$) of the last equation is zero, and, depending on k, the steady state solution of (4) is infinity ($k = 2$) or zero ($k = 1$).

4. DESCRIPTION OF THE ADAPTATION DYNAMICS

What does the adaptation dynamics defined by (1) to (6) look like? The process obviously integrates the activity generated by an input image $\mathcal{L}$, via the photoreceptor membrane potential P. The integration proceeds until P exceeds the threshold Θ. At this point, the integration process decelerates exponentially with a time constant $\tau_1 > 0$, since the corresponding solution to (4) is $\Theta(t) = \exp(-t/\tau_1)$. The dynamics of P is shown in Figure 4: luminance values that vary over 5 orders of magnitude are mapped onto roughly two orders of output magnitude in a way that contrast relationships of the input are preserved. Moreover, the process converges rather fast. Even for the smallest input intensities, convergence is reached at about 200 iterations. This fastness is a consequence of the dynamic switching process, which increases signal amplification G until P exceeds Θ (doing so reduces the integration time especially for weak luminance signals). Since this process (4) per se would grow in an unbounded fashion, one may question its physiological
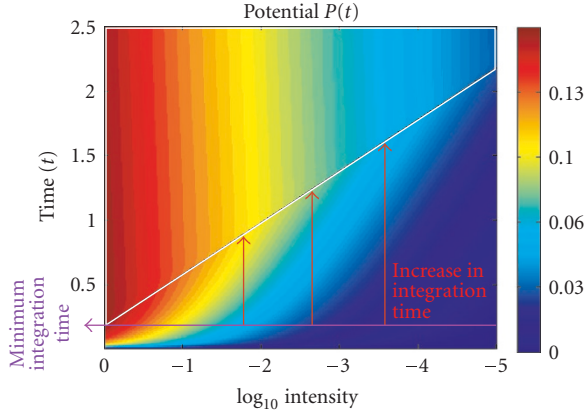
FIGURE 4: *Photoreceptor potential*: the photoreceptor potential P (1) is plotted as a function of time ($t = 0$ to 250 iterations) and input intensity ($\mathcal{L} \in \{10^0, 10^{-1}, \ldots, 10^{-5}\}$). The photoreceptor amplitude is color-coded (colorbar). "Convergence" occurs when the photoreceptor potential P exceeds a threshold Θ, and corresponds to the area over the diagonal line. The minimum integration time is delineated by the horizontal line at the bottom. With decreasing luminance, one observes an increase in integration time until "convergence" is reached (as illustrated by the red arrows pointing to the plateau). A similar increase in integration time with decreasing stimulus intensity levels is also known from the retina, and is expressed as Bloch's law of temporal integration. Bloch's law relates the threshold for seeing a stimulus to stimulus duration (i.e., integration time) and stimulus intensity: the product of stimulus duration and stimulus intensity equals a constant within a so-called critical time window. Bloch's law is especially prominent for scotopic vision.

plausibility. But as long as $\epsilon > 0$, or dynamically varying noise is present in the model, eventually all luminance values reach threshold in finite time, and as a consequence, G (4) switches from amplification to attenuation. This is to say that for $k = 2$, the process G is bounded mathematically from above. Furthermore, numerical experiments demonstrate that G does not adopt excessively high values (see Figure 5).[2]

Nevertheless, a suitably parameterized and asymptotically bounded process for substituting G, rather than a sharply cut exponential (as it is implemented by (4), (5), and (6)), would perhaps better reflect physiological reality—but for the moment we set aside plausible functions to keep the model concise.

Why should the threshold Θ drop with time? Imagine that we fix Θ to some constant value. In that case, all luminance values are integrated until they all reach the *same* threshold. This means that the integration process would establish a common level for bright and dark luminance values, what in the best of all cases would lead to a strong reduction of contrasts with respect to the input (Figure 3(c)). But there is yet another, more technical point, to this.

---

[2] If $P(t) \leq \Theta(t)$, the subthreshold gain obeys $G(t) = \exp(t/|\tau_2|)$. Assuming $t = 250$ iterations and using $|\tau_2| = 40.5$ (see Table 2) we get $G(t = 250) \approx 479.55$ as maximum amplification.
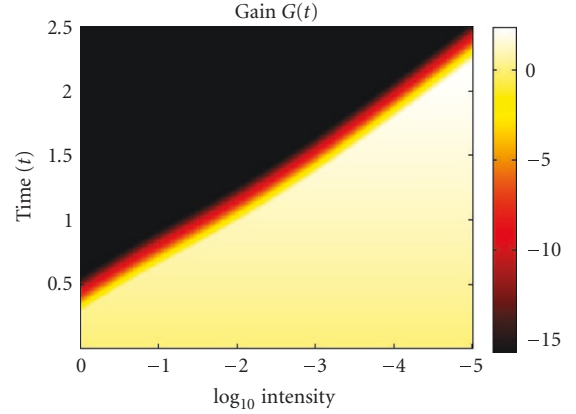

FIGURE 5: *Dynamics of the "switching" gain control*: the same as in Figure 4, but here the dynamics of the signal amplification variable $G(t, \mathcal{L})$ (4) is visualized. The bright (dark) area on the bottom (top) indicates where the gain control is switched on (off). Notice that the switching occurs rather fast around the red area. The switching area resembles a blurred line—compare it to the diagonal line delineating the convergence plateau in Figure 4.

Consider a pair of luminance values, one brighter than the other. Since the integration process proceeds with fixed time steps (and exponentially increasing gain), we may choose both luminance values such that they exceed the fixed threshold in a way that the previously dark luminance value leaves *more* super-threshold activity than the bright value (the brighter value must have exceeded threshold at some former time step, and thus its activity P already has decayed somewhat due to the passive leakage conductance g_{leak} in (1)). In other words, when decoding the photoreceptor potential P, the dark value would suddenly appear brighter than the original bright value. Such "contrast inversion" artifacts are avoided with a threshold that decreases with time. Thus, the dynamic threshold process (6) acts to preserve contrast polarities (notice that the threshold process asymptotically approaches zero).

Yet another type of artifact may emerge as a consequence of the exponentially increasing amplification signal G, most likely due to amplification of numerical noise while integrating the differential equations. With certain luminance distributions, especially with luminance ramps, step-like or ripple-like structures may appear when P is read out (of course the ripples are absent from the input, cf. Figure 2). Those artifacts are counteracted by the additional gain control mechanism (3). Its net effect is to continuously decrease the integration step size for (1) as the potential P grows. This effect gets especially prominent for high luminance values (see Figure 6).

5.   RESULTS OF NUMERICAL EXPERIMENTS

What should one expect from a "good" adaptation mechanism? It should map luminance values, which can be distributed over several orders of magnitude, onto a fixed target range of, say, one or two orders of magnitude. In this way,
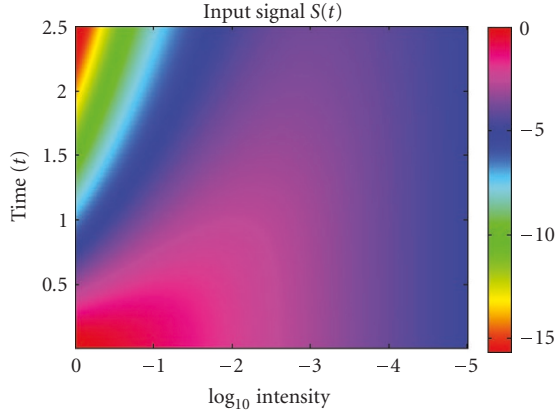
FIGURE 6: *Input signal*: the same as in **Figure 4**, but here the dynamics of the input signal $S(t, \mathcal{L})$ is visualized (3).

images with a high dynamic range could be visualized with a normal computer monitor. If we tried a direct visualization of a high dynamic range image without applying any adaptation, we could just see the luminance patterns of the first one or two orders of magnitude, while all smaller luminance values would be displayed in black (see **Figure 7**; notice that the optic nerve has a similar transmission bandwidth). Additionally, a "good" adaptation mechanism should leave an input image unchanged which does only vary over one or two orders of magnitude. Or at least leave such an image unchanged as far as possible. Contrast strength should ideally be preserved. Put another way, compression effects that are introduced by the adaptation mechanism should be minimized.

We compare the results of our mechanism with one proposed in [19, 20] (subsequently denoted by "Grossberg and Hong").[3]

In order to assure that, at some time, $P(t)_{ij} > \Theta(t)$ at all positions (i, j), zero values of the original luminance distribution were substituted by the half of the second smallest luminance value, that is, $\epsilon = 0.5 * \min\{\mathcal{L}_{ij} : \mathcal{L}_{ij} > 0\}$, if not otherwise stated. We used standard benchmark images of size 256×256 pixels as inputs $\mathcal{L}$.

Figure 8 shows the results with the MIT image, where the result obtained with our method is slightly less saturated than the one obtained with Grossberg and Hong's method.

In order to better explore the performance of the two methods, we superimposed the original test images with artificially generated illumination patterns. In **Figure 9**, the MIT image was multiplied with a luminance ramp to simulate an illumination gradient. In the latter case, the result from Grossberg and Hong is less saturated than ours.

In **Figure 7**, the original image (shown in **Figure 11**) was subdivided in four "tiles," where within each tile luminance values vary over a different order of magnitude. This test

---

[3] We implemented [20, equations (A3) to (A8)], and integrated their model over 500 iterations with Euler's method, where a integration step size of 0.01 was used.
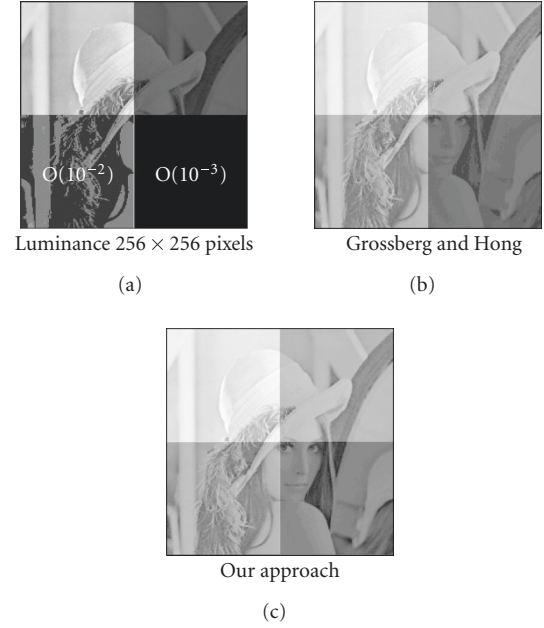

FIGURE 7: *Tiled Lena image*: the original Lena image (with luminance values between 0 and 1, see **Figure 11**) was subdivided into four tiles, and tiles were multiplied with 10^0, 10^{-1}, 10^{-2}, and 10^{-3}, respectively. In the input (a), both of the lower tiles are displayed in black. The order of magnitude of the corresponding luminance range is indicated with the black tiles.
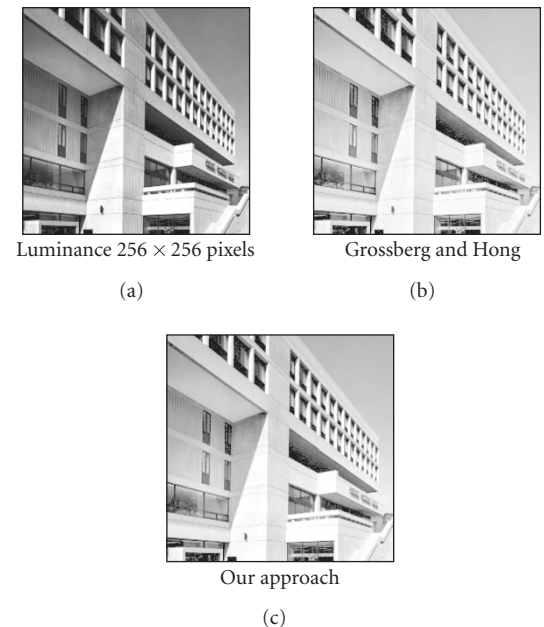

FIGURE 8: *MIT image*: (a) shows the input image, with luminance values originally varying from 0 to 255. The input image was normalized such that the maximum intensity value was 1, and the minimum 0. Subsequently, all zero luminance values were substituted by $\epsilon = (1/255)/2$. (b) shows the result obtained with the method described in [19, 20] (500 iterations). (c) was obtained with our approach (150 iterations; convergence occurred within simulation time). Both (b) and (c) show the cone's membrane potential.

Luminance 256 × 256 pixels

(a)

Grossberg and Hong
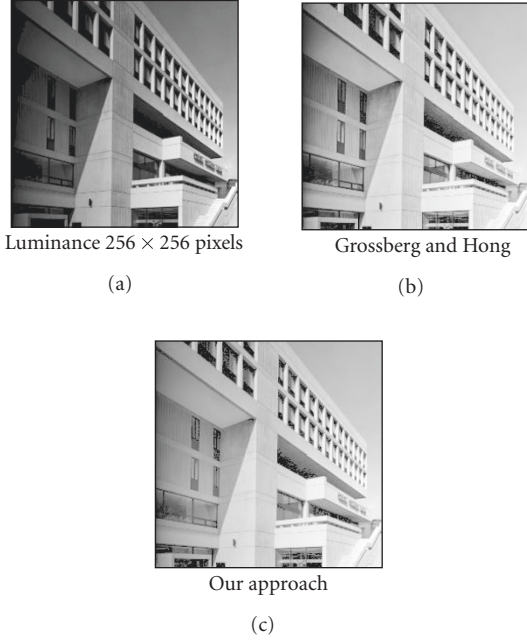
(b)

Our approach

(c)

FIGURE 9: *MIT image with overlying luminance ramp*: the original MIT image (see Figure 8) was multiplied with a luminance ramp which linearly increases from left (intensity 0) to the right (intensity 1).

Luminance 256 × 256 pixels

(a)
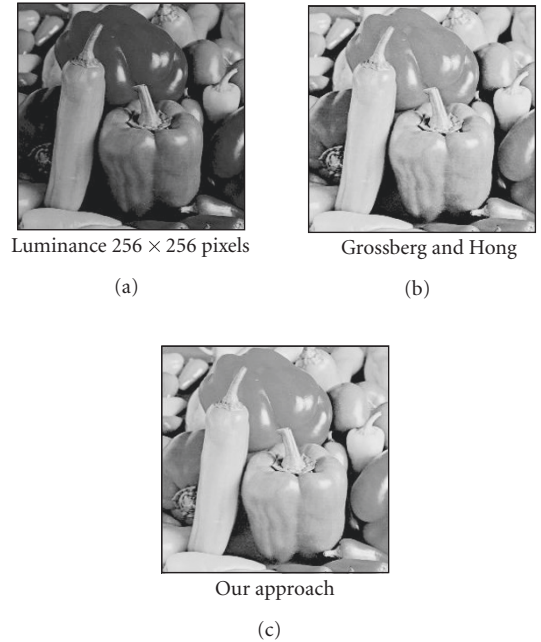

Grossberg and Hong

(b)

Our approach

(c)

FIGURE 10: *Power-law-stretched Peppers image*: luminance values of the original Peppers image (see Figure 11) were raised to the power of 4 to create a high dynamic range image.

image mimics a situation where the range of luminance values within a scene varies over four orders of magnitude. Both methods push luminance values sufficiently high such that details in the darkest tile are rendered visible (where our method yields an overall more brighter result—and hence the darkest patch is better visible). Thus, four orders of magnitude of input range are mapped onto two orders of magnitude available for visualization, a situation that is similar to situations which are met by the retina.

In the last example, we created an artificial high dynamic range image (Figure 10) from the original "Peppers" image (Figure 11). In this case, our method produces a slightly brighter result compared with Grossberg and Hong: the result generated with Grossberg and Hong's method has harder contrasts.

We conducted further simulations where we set $\mathcal{L}_{ij} \leftarrow P_{ij}$ after convergence, and restarted the simulation. The results did not change, indicating that the model's state after converging the first time already corresponds to a steady state solution.

6. MODEL BEHAVIOR WITH PARAMETER CHANGES

The parameters of our model can be tuned according to the expected numerical range of luminance values. In this way, compression effects in the output are reduced, which can lead to the generation of visually more pleasing results.

Increasing the value of γ (Table 2; (3)) reduces the overall compression of the input at the cost of low-intensity regions. This is to say that low-intensity regions will appear darker, and regions with higher intensities will be rendered with

(a)

(b)
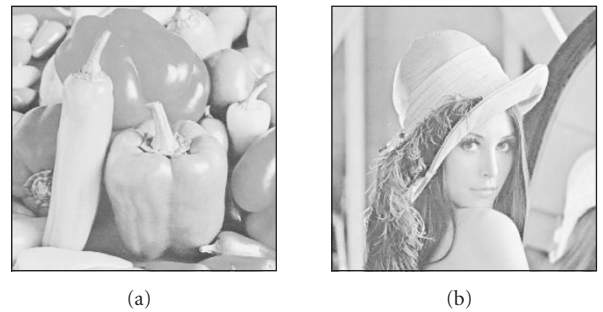
FIGURE 11: *Original "Lena" and "Peppers" image*: these images are shown for comparing them with the results presented in Figures 7 and 10, respectively.

somewhat improved contrasts. A similar effect results, albeit more intense, when increasing the threshold decay time constant τ_Θ (6). Decreasing the initial threshold value Θ_0 (6) will slightly increase overall brightness and compression, respectively. The model behavior is quite robust against changes in the damping time constant τ_1, since this mechanism is backed up by the signal gain control stage (3). Nevertheless, variations in the value of the amplification time constant τ_2 bear strongly on the results: a decrease improves greatly the adaptation behavior, but if τ_2 is set too low artifacts may occur, such as contrast polarities being reversed with respect to the input. On the other hand, if $\tau_2 \rightarrow \infty$, no adaptation at all takes place. In future versions of our approach, this influential parameter could be set automatically as a spatially varying function of the structures in the input image.

7. THIS THING CALLED "EPSILON"

As it turned out, a "smart" choice of ϵ can even improve the contrasts in the visualization of the results. Because for displaying, each image is normalized to occupy the full range of available gray levels, if ϵ is too small with respect to the second smallest luminance value, it gets not sufficiently pushed by the adaptation process, such that in the adapted image the difference between the smallest and the second smallest value is too big. As a consequence, many of the darker gray levels are not used (if we assume a linear mapping of activity to gray levels), what leaves less gray levels for displaying the other (higher) luminance values. Hence, the contrasts in the displayed image will be reduced. Ideally, ϵ should depend in some way on how dark the input image is perceived by a human observer. Finding an adequate function that automatically sets the value of ϵ would be an interesting topic for future research.

8. DISCUSSION AND CONCLUSIONS

We presented a novel theory about the adaptational mechanisms in retinal photoreceptors. Our theory is abstract in the sense that we did not attempt to identify model stages with components of the phototransduction cascade (as outlined in Section 2). Nevertheless, one is tempted to draw corresponding parallels between our model and physiological data. In the transduction cascade, there are (at least) two sites of amplification: the serial activation of transducins by the active form of rhodopsin Rh*, and the hydrolysis of cGMP by phosphodiesterase. An amplification of the signal takes also place in our model by virtue of G in (4). Furthermore, Ca^{2+} constitutes a messenger for adaptation. In contrast, there is no corresponding variable for describing the concentration of Ca^{2+} in our model. Nevertheless, the membrane potential P subserves two different purposes. First, it corresponds to the output of the photoreceptor. Second, it constitutes a feedback signal that acts to control signal amplification—and hence the adaptation process. As Ca^{2+} is known to be linearly related to the membrane potential, it seems reasonable to consider P as a lumped-together description for both the membrane potential and the Ca^{2+} concentration.

Indeed, one can draw further parallels. In our model, signal amplification stops as soon as the membrane potential exceeds a threshold, in order to counteract saturation effects (5). This process is reminiscent on the binding of arrestin to phosphorylated Rh*, leading to a complete inactivation of the photopigment, and thus to a ceasing of the transduction cascade.

In our model, there is yet another way to counteract saturation effects, by means of the divisive inhibition stage (3). This process can be compared to the interaction of Ca^{2+} with the visual cycle, which causes an acceleration of the rate of Rh* phosphorylation [36–38]. This interaction is brought about by the Ca^{2+}-binding protein recoverin, and decreases the lifetime of Rh*. As a consequence, less cGMP will be hydrolyzed upon absorption of a photon [26].

On the technical side, computer simulations demonstrated that our approach is on a par with a recently proposed model by Grossberg and Hong [19, 20] "(G&H)." However, several crucial differences exist between their approach and ours.

First and above all, the critical stage for adaptation in Grossberg and Hong's approach consists of the feedback provided by electrically coupled horizontal cells. Light adaptation through the outer segment can be decoupled from the actual adaptation dynamics, and hence may be considered as a preprocessing step in their model.

Remarkably, our approach achieves similar adaptation results *without* incorporating the horizontal-to-cone feedback loop. This prediction is consistent with physiological data, as cone photoreceptors can decrease their sensitivity over about 8 log units of background intensity [15]. Moreover, feedback from horizontal cells may even further improve adaptation. Since we have seen, on the other hand, that contrasts are reduced as a consequence of the dynamic range compression, one may speculate that feedback from horizontal may also compensate for this effect, by reenhancing contrasts. Notice that contrast enhancement is tantamount to center-surround interactions. Because adjacent horizontal cells of the same type are fused by gap junctions, their feedback will influence the membrane potential of neighboring cones within some radius of the actually stimulated photoreceptor. In this way, the antagonistic receptive field structure is created in bipolar cells. But then bipolar cells represent a contrast-enhanced signal of the photoreceptors. Therefore, neurophysiological data are consistent with our ideas.

Both models have similar complex with respect to parameter spaces. Grossberg and Hong's approach has some 10 parameters, whereas ours has 7 (plus the ϵ). Although we did not carry out a detailed analysis of computational complexity, the respective model structures suggest that the Grossberg and Hong model is computationally more demanding. The latter fact seemed to be confirmed with our simulations on a serial computer, where our model converged in a fraction of the time that was necessary to achieve comparable results with the Grossberg and Hong model.[4]

Similar to the Grossberg and Hong model, another approach [39] is also motivated by the observation that strong contrasts usually indicate reflectance changes in natural scenes, as opposed to intensity variations due to changes in illumination. The approach in [39], however, has no stage for luminance adaptation, and only computes an "anisotropically like" smoothed version of the image, which is used for exerting divisive gain control directly on intensity values (cf. Table 1). The lateral connectivity between cells that form the diffusion layer is controlled by inverse Weber contrasts. Hence, both strong and weak contrasts in the original image may affect the degree of smoothing. Simulation results obtained with our implementation of Gross' and

---

[4] In our implementation of the Grossberg and Hong model we used the steady state equations where possible, and also the long-range diffusion mechanism is as proposed by the authors.

Brajovic's approach revealed strong boundary enhancement if tuned such that the adaptation was comparable to the other two methods. This suggests that the signal transduction characteristics of Gross' and Brajovic's approach are high-pass.

Our model, perhaps with different parameter values, should as well be useful for displaying high dynamic range images, or synthetic aperture radar images. This is a topic that will be pursued with future research. Further interesting questions address the incorporation of feedback from horizontal cells, and possibly of reset mechanisms for the threshold process, in order to extend our model's processing capacities to image sequences.

ACKNOWLEDGMENTS

REFERENCES

[1] J. Walraven, C. Enroth-Cugell, D. Hood, D. MacLeod, and J. Schnapf, "The control of visual sensitivity: receptoral and postreceptoral processes," in *The Neurophysiological Foundations of Visual Perception*, L. Spillman and J. Werner, Eds., pp. 53–101, Academic Press, New York, NY, USA, 1990.

[2] H. Barlow and W. Levick, "Threshold setting by the surround of cat retinal ganglion cells," *Journal of Physiology, London, B*, vol. 212, p. 1, 1976.

[3] D. Hood and M. Finkelstein, "Sensitivity to light," in *Handbook of Perception and Visual Performance, Volume 1: Sensory Processes and Perception*, K. Boff, L. Kaufman, and J. Thomas, Eds., chapter 5, pp. 5.1–5.66, John Wiley & Sons, New York, NY, USA, 1986.

[4] V. Mante, R. A. Frazor, V. Bonin, W. S. Geisler, and M. Carandini, "Independence of luminance and contrast in natural scenes and in the early visual system," *Nature Neuroscience*, vol. 8, no. 12, pp. 1690–1697, 2005.

[5] J. H. van Hateren, "Processing of natural time series of intensities by the visual system of the blowfly," *Vision Research*, vol. 37, no. 23, pp. 3407–3416, 1997.

[6] G. Martin, "Schematic eye models in vertebrates," *Progress in Sensory Physiology*, vol. 4, p. 44, 1983.

[7] R. Shapley and C. Enroth-Cugell, "Visual adaptation and retinal gain controls," *Progress in Retinal Research*, vol. 3, pp. 263–346, 1984.

[8] S. B. Laughlin, "The role of sensory adaptation in the retina," *Journal of Experimental Biology*, vol. 146, pp. 39–62, 1989.

[9] R. Normann, I. Perlman, and P. Hallet, "Cone photoreceptor physiology and cone contributions to colour vision," in *Vision and Visual Dysfunction, The Perception of Colour*, P. Gouras, Ed., pp. 146–162, Macmillan Press, London, UK, 1991.

[10] H. B. Barlow, "The Ferrier Lecture, 1980. Critical limiting factors in the design of the eye and visual cortex," *Proceedings of the Royal Society of London. Series B. Biological Sciences*, vol. 212, no. 1186, pp. 1–34, 1981.

[11] D. C. Hood, "Lower-level visual processing and models of light adaptation," *Annual Review of Psychology*, vol. 49, pp. 503–535, 1998.

[12] M. Meister and M. J. Berry II, "The neural code of the retina," *Neuron*, vol. 22, no. 3, pp. 435–450, 1999.

[13] I. Fahrenfort, R. L. Habets, H. Spekreijse, and M. Kamermans, "Intrinsic cone adaptation modulates feedback efficiency from horizontal cells to cones," *Journal of General Physiology*, vol. 114, no. 4, pp. 511–524, 1999.

[14] G. L. Fain, H. R. Matthews, M. C. Cornwall, and Y. Koutalos, "Adaptation in vertebrate photoreceptors," *Physiological Reviews*, vol. 81, no. 1, pp. 117–151, 2001.

[15] D. A. Burkhardt, "Light adaptation and photopigment bleaching in cone photoreceptors in situ in the retina of the turtle," *Journal of Neuroscience*, vol. 14, no. 3 I, pp. 1091–1105, 1994.

[16] J. Dowling, *The Retina: An Approachable Part of the Brain*, Belknap Press/Havard University Press, Cambridge, Mass, USA, 1987.

[17] H. Kolb, E. Fernandez, and R. Nelson, "Webvision. The organization of the vertebrate retina," 2000, http://retina.umh.es/Webvision.

[18] M. E. Burns and D. A. Baylor, "Activation, deactivation, and adaptation in vertebrate photoreceptor cells," *Annual Review of Neuroscience*, vol. 24, pp. 779–805, 2001.

[19] S. Grossberg and S. Hong, "Cortical dynamics of surface lightness anchoring, filling-in, and perception," *Journal of Vision*, vol. 3, no. 9, p. 415a, 2003.

[20] S. Hong and S. Grossberg, "A neuromorphic model for achromatic and chromatic surface representation of natural images," *Neural Networks*, vol. 17, no. 5-6, pp. 787–808, 2004.

[21] G. A. Carpenter and S. Grossberg, "Adaptation and transmitter gating in vertebrate photoreceptors," *Journal of Theoretical Neurobiology*, vol. 1, pp. 1–42, 1981.

[22] M. Kamermans, I. Fahrenfort, K. Schultz, U. Janssen-Bienhold, T. Sjoerdsma, and R. Weiler, "Hemichannel-mediated inhibition in the outer retina," *Science*, vol. 292, no. 5519, pp. 1178–1180, 2001.

[23] T. D. Lamb, "Spatial properties of horizontal cell responses in the turtle retina," *Journal of Physiology*, vol. 263, no. 2, pp. 239–255, 1976.

[24] M. Piccolino, J. Neyton, and H. M. Gerschenfeld, "Decrease of gap junction permeability induced by dopamine and cyclic adenosine $3' : 5'$-monophosphate in horizontal cells of turtle retina," *Journal of Neuroscience*, vol. 4, no. 10, pp. 2477–2488, 1984.

[25] P. Perona and J. Malik, "Scale-space and edge detection using anisotropic diffusion," *IEEE Transactions on Pattern Analysis and Machine Intelligence*, vol. 12, no. 7, pp. 629–639, 1990.

[26] P. D. Calvert, V. I. Govardovskii, V. Y. Arshavsky, and C. L. Makino, "Two temporal phases of light adaptation in retinal rods," *Journal of General Physiology*, vol. 119, no. 2, pp. 129–145, 2002.

[27] R. J. Perry and P. A. McNaughton, "Response properties of cones from the retina of the tiger salamander," *Journal of Physiology*, vol. 433, no. 1, pp. 561–587, 1991.

[28] P. D. Calvert, T. W. Ho, Y. M. Lefebvre, and V. Y. Arshavsky, "Onset of feedback reactions underlying vertebrate rod photoreceptor light adaptation," *Journal of General Physiology*, vol. 111, no. 1, pp. 39–51, 1998.

[29] T. I. Rebrik and J. I. Korenbrot, "In intact mammalian photoreceptors, Ca^{2+}-dependent modulation of cGMP-gated ion channels is detectable in cones but not in rods," *Journal of General Physiology*, vol. 123, no. 1, pp. 63–75, 2004.

[30] C. F. Vaquero, A. Pignatelli, G. J. Partida, and A. T. Ishida, "A dopamine- and protein kinase A-dependent mechanism for network adaptation in retinal ganglion cells," *Journal of Neuroscience*, vol. 21, no. 21, pp. 8624–8635, 2001.

[31] R. Weiler, K. Schultz, M. Pottek, S. Tieding, and U. Janssen-Bienhold, "Retinoic acid has light-adaptive effects on horizontal cells in the retina," *Proceedings of the National Academy of Sciences of the United States of America*, vol. 95, no. 12, pp. 7139–7144, 1998.

[32] D. Green, J. Dowling, I. Siegal, and H. Ripps, "Retinal mechanisms of visual adaptation in the skate," *The Journal of General Physiology*, vol. 65, no. 4, pp. 483–502, 1975.

[33] H. B. Barlow and W. R. Levick, "Changes in the maintained discharge with adaptation level in the cat retina," *Journal of Physiology*, vol. 202, no. 3, pp. 699–718, 1969.

[34] S. M. Smirnakis, M. J. Berry, D. K. Warland, W. Bialek, and M. Meister, "Adaptation of retinal processing to image contrast and spatial scale," *Nature*, vol. 386, no. 6620, pp. 69–73, 1997.

[35] T. Hosoya, S. A. Baccus, and M. Meister, "Dynamic predictive coding by the retina," *Nature*, vol. 436, no. 7047, pp. 71–77, 2005.

[36] S. Kawamura, "Rhodopsin phosphorylation as a mechanism of cyclic GMP phosphodiesterase regulation by S-modulin," *Nature*, vol. 362, no. 6423, pp. 855–857, 1993.

[37] C.-K. Chen, J. Inglese, R. J. Lefkowitz, and J. B. Hurley, "Ca^{2+}-dependent interaction of recoverin with rhodopsin kinase," *Journal of Biological Chemistry*, vol. 270, no. 30, pp. 18060–18066, 1995.

[38] V. A. Klenchin, P. D. Calvert, and M. D. Bownds, "Inhibition of rhodopsin kinase by recoverin. Further evidence for a negative feedback system in phototransduction," *Journal of Biological Chemistry*, vol. 270, no. 27, pp. 16147–16152, 1995.

[39] R. Gross and V. Brajovic, "An image preprocessing algorithm for illumination invariant face recognition," in *Audio-and Video-Based Biometrie Person Authentication (AVBPA '03)*, J. Kittler and M. Nixon, Eds., vol. 2688 of *Springer Lecture Notes in Computer Sciences*, pp. 10–18, Guildford, UK, June 2003.

Matthias S. Keil holds a degree in physics from the University of Bayreuth, Germany, and a degree in neural computation from the Ruhr University of Bochum, Germany. He received his Ph.D. degree in 2003 from the University of Ulm, Germany for proposing and modeling neuronal circuits underlying human brightness perception. He participated in several European projects. His research interests are the information processing in the brain, applying neuronal models to image processing, and complex dynamical systems. He is currently a Postdoctoral Fellow at the Computer Vision Center at the Autonomous University of Barcelona (UAB), Barcelona, Spain.

Jordi Vitrià received the Ph.D. degree from the Autonomous University of Barcelona (UAB), Barcelona, Spain, for his work on mathematical morphology, in 1990. He joined the Computer Science Department, UAB, where he became an Associate Professor in 1991. His research interests include machine learning, pattern recognition, and visual object recognition. He is the author of more than 40 scientific publications and one book.